

Microscopic Description of Super Heavy Nuclei

Y. K. Gambhir^a, A. Bhagwat^a and M. Gupta^{a,b}

^a Department of Physics, I.I.T. Powai, Bombay 400076, India,

^b Manipal Academy of Higher Education, Manipal 576119, India

The results of extensive microscopic Relativistic Mean Field (RMF) calculations for the nuclei appearing in the α - decay chains of recently discovered superheavy elements with $109 \leq Z \leq 118$ are presented and discussed. The calculated ground state properties like total binding energies, Q values, deformations, radii and densities closely agree with the corresponding experimental data, where available. The root mean square radii closely follow $A^{1/3}$ law (A being the mass number) with the constant $r_o = 0.9639 \pm 0.0005$ fm. The double folding ($t\rho\rho$) approximation is used to calculate the interaction potential between the daughter and the α , using RMF densities along with the density dependent nucleon - nucleon interaction (M3Y). This in turn, is employed within the WKB approximation to estimate the half lives without any additional parameter for α - decay. The half lives are highly sensitive to the Q values used and qualitatively agree with the corresponding experimental values. The use of experimental Q values in the WKB approximation improves the agreement with the experiment, indicating that the resulting interaction potential is reliable and can be used with confidence as the real part of the optical potential in other scattering and reaction processes.

1. Introduction

The synthesis of the superheavy elements (SHE) is a subject that has remained at the forefront of nuclear physics ever since the prediction of islands of stability in this mass region ($Z \sim 114$, $N \sim 184$) in the 1960's [1, 2]. After about four decades of experimentation, it still does not seem to be possible to reach the $N = 184$ closed shell with stable neutron rich beams such as ^{48}Ca used at JINR/Dubna. In order to get closer, radioactive ion beams with neutron excess higher than ^{48}Ca will be required [3] such as those that may become available with the DRIBs facility at Dubna [4] and elsewhere.

We start with a short review of the current status of experimental work in Section II, followed by a brief description of the theoretical framework in Section III. The results and discussion are contained in section IV. The conclusions are presented in the last (V) section.

2. Status of Experimental Work

The elements above Fermium have been created in the laboratory by completely fusing heavy ions. The evaporation residues (EVR's) of compound nuclei (CN) upto about $Z = 112$ are produced primarily by successive alpha - decays to known nuclei enabling

their unambiguous identification by the method of $\alpha - \alpha$ correlations [5]. However, at Seaborgium, the production cross - sections fall below one nanobarn with half - lives of less than a second. To access the new region above $Z=106$, new methods had to be devised [6, 7] such as ‘cold-fusion’ using Pb and Bi targets [8], invented by the Dubna Group and successfully used in the early discoveries of Bh, Hs and Mt. Together with increasingly sensitive detection methods it thus became possible to identify a single atom [9]. Using such techniques, two isotopes of Hassium, $^{264,265}\text{Hs}$ were created at GSI in the 1980’s [10, 11], ^{267}Hs in the mid - 90’s at Dubna [12] and ^{277}Hs as a part of the $Z = 114$ chain [13] also at Dubna. The GSI group had successfully produced the elements ^{270}Ds [14], $^{269,271}\text{Ds}$, $^{272}\text{111}$, [15, 16, 17, 18], by 1998 and $^{277}\text{112}$ [19] by the year 2002. Additionally, two decay chains have come from LBNL confirming the ^{271}Ds data from GSI using the same $^{208}\text{Pb}(^{64}\text{Ni},n)$ reaction [20] but with gas-filled detectors to enhance EVR collection. In the last couple of years new results have become available from RIKEN for $^{271}\text{110}$ [21, 22], $^{272}\text{111}$ [23] and for $^{278}\text{113}$ [24]. With extensive activity underway at this facility, the current experimental program includes the on - going cold fusion synthesis of recently completed experiments for $^{277}\text{112}$ and future plans for $^{283}\text{114}$ [25]. Thus, cold fusion reactions usually involving the evaporation of one neutron, have successfully been used to synthesize elements up to $Z=112$. However the maximum production cross-section for this element ($Z = 112$) is achieved at an excitation energy of only ~ 10 MeV. If one were to extrapolate, to reach the heavier elements the excitation energy at the Coulomb barrier may well drop below zero (see [26] for an exhaustive discussion). Clearly, as one approaches the predicted island of stability at $N=184$ (assuming the correctness of this postulate), a higher excitation energy is required. This is achievable through greater neutron excess in both the target and the projectiles as with ‘hot fusion’ reactions. The Dubna group have successfully used actinide targets with a ^{48}Ca beam to fuse $Z \geq 114$, where the compound nucleus is formed following the evaporation of three or more neutrons. Elements $^{286,287,288,289}\text{114}$, $^{287,288}\text{115}$ and $^{290,291,293}\text{116}$ have thus been produced at higher excitation energies and different cross-sections [27, 28, 29, 30]. Preliminary results for $^{294}\text{118}$ from a single event have also been cited [31] with further experimentation in progress. As a final observation, even with hot fusion reactions, EVR’s may not pass through a region greater than $N=174\text{--}177$ [32]. Though this is closer by about 6-8 neutrons to the $N=184$ region, it may not be sufficient. It is hoped that with the dawn of the new era of radioactive ion beams the ‘sea of instability’ may be breached.

From the above discussion, it is clear that above $Z=112$, especially in reactions involving neutron rich beams of the rare ^{48}Ca isotope, α -decay chains do not end with known nuclei making the method of $\alpha - \alpha$ correlations insufficient for the unambiguous identification of isotopes. That these chains would end in unknown regions is easily understood when recognizing that with each successive α (or β -decay), daughter nuclei move away from the regions of stability and spherical closed shells towards instability. It is reasonable to expect spontaneous fission (SF) to become the preferred decay mode over others. SF could then be considered to be a reliable signature for the formation of extremely heavy nuclei [33]. In such cases, and ideally suited to single atom production, chemical methods provide for excellent assignment criteria if the half-lives are within the range of detection i.e. around a few seconds, with cross-sections less than 100 pb following genetically established decays [34]. Generally, cold fusion experiments produce nuclei with shorter half-lives than those

synthesized by hot fusion. Hot fusion reactions are thus more suitable for chemical studies. Analogies may be drawn between the chemical properties of compounds of unknown Z with those of the chemical type of known elements allowing for specific assignments [35]. By adopting quick and sensitive techniques for separation, it has been possible to study Rf, Db, Sg and Bh (see [36] for a complete review of chemistry). Furthermore, as α -decay may be considered to be the signature mechanism for the unique identification of each nuclide, genetic correlations are unambiguous. The detection of an α or a SF fragment is the only means for detecting a single atom following chemical separation which can be done with high efficiency. The method was used very effectively in confirming the α -decay grand-daughters for $^{277}112$ synthesized at GSI, when 7 decay chains from Hs isotopes were unambiguously identified after chemical separation [37]. First attempts to study the chemistry of $Z = 112$ were made by fusing natural U with a ^{48}Ca beam to form $^{283}112$ [38, 39, 40]. Due to various problems with the experimental set-up these results are still tentative and further experiments are underway [41].

Where even shorter decay half-lives occur and as production cross - sections get smaller, still other techniques have been devised. Investigations wherein masses from evaporation residues (EVR's) are identified by exploiting the dependence of production cross-sections on excitation energy (thus defining the neutron yield) together with cross-bombardments in which the mass number of either the projectile or target is varied (thus changing the relative yield of resulting xn -evaporation channels) have been successfully carried out in the past. The methods find their use in both the identification of unknown nuclei as well as in the study of those with short SF decay half-lives [35]. This is best illustrated in the case of $Z = 114$ and $Z = 116$, where when re-visiting results from earlier experiments using more stringent methods, the Russian collaborations revised their previous conclusions resulting in re-assignments [30] for $^{286,287,288,289}114$, $^{290,291,292,293}116$ [42]. These experiments have been carried out using the Dubna Gas Filled Recoil Separator in 'hot fusion' reactions involving $^{233,238}\text{U}$, ^{242}Pu and ^{248}Cm targets, collectively described in [42]. Other isotopes identified and discussed therein include ^{267}Rf , ^{271}Sg , ^{275}Hs , $^{279,281}\text{Ds}$, and $^{282-285}112$. It is expected that existing contradictions in the case of $^{287}114$ and $^{283}112$ will be resolved via continuing hot fusion studies along similar lines in the immediate future. Even these methods have their limitations where the use of cross-reactions and different decay channels become increasingly difficult with rapidly diminishing cross-sections for higher Z .

It is clear that the direct determination of Z requires a stringent mass resolution a few mass units $\approx 1\%$ to measure the difference between a xn and an αxn evaporation channel for instance. The mass resolution should in fact be better than 1 amu at the level of 300 amu ($\Delta m/m < 0.3\%$) [43, 44]. It is interesting that for all atoms heavier than U, masses have not been measured. This is due to the inherently small separation efficiency of elements in the range $89 \leq Z \leq 103$. The identification of nuclei produced using in-flight recoil separators to date is based on the kinematic characteristics of the recoil products - the energy of the recoils and the emission angle with respect to beam direction. The necessity to retain the kinematic properties of the heavy elements being studied imposes conditions on target thickness, background conditions and relatively poor (factor of ~ 6) suppression of reaction by-products [45]. New generation "isotope separator on-line" (ISOL) based machines such as 'MASHA' (Mass Analyzer for Superheavy Atoms) coming

up at JINR-Dubna will be able to directly determine the mass of separated atoms in the range $112 \leq Z \leq 120$. The limitation on measurement is set by the shortest measurable half-life, $T_{1/2} \sim 0.5$ s [46]. MASHA is expected to be operational shortly and this will open up new avenues for the study of the chemical properties of the SHE.

3. Status of Theory

As experimental methods have advanced considerably over the last couple of decades, several theoretical formulations have been developed and employed to describe the ground state properties of each of the nuclei along the α - decay chains including binding energies, Q_α values etc. In spherical even-even nuclei, alpha transitions are expected to go from ground state to ground state and hence alpha decay energies (Q-values) serve as a sensitive signature for local changes in stability. This is not quite so clear in the case of deformed doubly even nuclei where transitions may originate from low lying rotational levels [47] or odd nuclei where transitions may be greatly hindered and spin isomerism may occur.

Whereas observed Q-values may, in general, be measured quite accurately, uncertainties do exist in experimental half-lives. Cross-section limits were already less than 12 pb for the creation of Ds and Z=111, for instance [48, 49] and dropped to about 1 pb for the Element 112 [15], resulting in poor statistics offered by single-atom count-rates. Interestingly, it is seen that α -decay half-lives are not as precise as one may think in microscopic calculations either: small variations in Q-values (to within a couple of hundred keV) dramatically affect theoretical estimates of half-lives. Given this imprecision in observed half-lives, they cannot be used in themselves for experimental assignments. However, a relatively long half-life *in the presence of* a high Q_α -value, serves as a strong indicator for elements $Z > 100$ [35]. Furthermore, longer T_α 's for even-even nuclei would imply higher hindrance factors, thereby serving to exclude the expected ground-to-ground transitions in such cases. Since the experimental presence of such hindrance factors could be considered as a property for assignment (or its exclusion) [35], theoretical predictions and comparisons will serve as a valuable guide. Finally, the qualitative trend of Q-values over say, neutron numbers, could serve as a good indication of the transition from deformation to sphericity as one traverses the neighborhood of N=162 shell and goes towards the spherical Z=114 region. It is important that such arguments be kept in mind when comparing calculations with experiment.

Several theoretical investigations have been carried out using the microscopic - macroscopic (MicMac) method and the self consistent mean field in both the relativistic and non relativistic formalisms. The primary aim in early studies has been to predict the combination of neutron number (N) and proton number (Z) where spherical shell closure may occur. An "island of stability" had been predicted around the hypothetical doubly magic $^{298}_{114}$ (N=184) about 30 years ago. More recently, nuclei in this vicinity are expected to be spherical or almost so with longer half-lives. Most theories do predict N=184 as being magic, however, there is no consensus on the location of the proton magic number due to differences in the treatment of the large Coulomb term and the spin-orbit interaction. MicMac models, which assume a prior knowledge about the densities and single particle potentials, include the Finite Range Droplet Model with folded Yukawa single particle potentials (FRDM+FY) [50] and the Yukawa plus Exponential model with Woods-Saxon

single particle potentials (YPE+WS) [51, 52], both of which confirm the prediction of $^{298}_{114}_{184}$ as being the next spherical doubly-magic nucleus. Non relativistic microscopic models such as the Skyrme-Hartree-Fock-Bogoliubov method [53] where the spin-orbit term has to be manually introduced, predict $Z=120$ may be as probable as $Z=114$, indicating that magic shells in this region are isotope dependent [54, 55]. Such techniques tend to overestimate the splitting of levels due to the spin-orbit coupling which may effect predictions for shell closures. With the large density of single particle states which in turn characterizes this mass region, the SHE serve as a sensitive probe for distinguishing between the various theories that attempt to predict shell structure, especially when these models describe stable nuclei with comparable accuracy. Also, it has been known for some time that deformation effects are important to the understanding of stability in this region [53]. Bohr and Mottelson have observed that deformation may enhance stability [56].

Relativistic Mean Field theories (RMF) which incorporate the spin-orbit term naturally, [57, 58, 59, 60, 61, 62, 63, 64] generally do better than the non-relativistic MF models. RMF has been very successful in describing ground state (g.s.) properties for nuclei spanning the entire periodic table, thereby claiming a ‘global fit’ [61, 64, 65]. This method has also been applied successfully [66, 67, 68, 69, 70, 71, 72, 73, 74, 75] to describe the ground states of these super-transactinides where both pairing effects and deformation play an important role. However, it is known that in all self-consistent models the occurrence of a spherical proton (neutron) shell closure with a given Z (N) can change with varying neutron number N (Z). Using the RMF formalism, neutron number $N=162$ has been predicted [66] to exhibit shell closure at around $Z = 108 - 110$. This is consistent with the findings of [76]. In addition, the calculated shell corrections (see Tab.5, page 222 of [66]) peak at $N = 166$ for $Z = 112$ indicating a stability for $Z = 112$ around $N = 166$, in agreement with experimental observations of the superheavy nucleus $^{277}_{112}$.

In this work we present comprehensive and systematic calculations for experimentally observed chains of SHE in the region $109 \leq Z \leq 118$. Binding energies, deformations, Q -values, radii and densities are calculated for the ground states and compared with the corresponding experimental values where available. The calculations agree well with the experiment. Most of the earlier investigations have been devoted to the description of the g.s. properties of SHE. Here, we focus on calculating their half lives.

The calculated RMF densities are used to derive the projectile-daughter interaction energy using the Double Folding (DF) model with the density dependent M3Y (DDM3Y) effective nucleon-nucleon interaction. This in turn is used to calculate the α -decay half life of the parent nucleus using the WKB approximation [72, 75].

3.1. Relativistic Mean Field Theory

The Relativistic Mean Field (RMF) theory [61, 64] is now established to be one of the most successful approach for the accurate description of nuclear properties. It starts with a Lagrangian describing the Dirac spinor nucleons interacting via exchange of mesons and the photon. The mesons considered here are: the isoscalar - scalar σ , isoscalar - vector ω and isovector - vector ρ mesons. The σ (ω) meson produces long range attraction (short range repulsion), whereas the ρ meson is necessary for the isospin dependence of the nuclear properties. The photon, as usual, produces the Coulomb interaction. The

Lagrangian consists of free baryon and meson terms and the interaction terms. The Euler - Lagrange variational principle yields the equations of motion. In the mean field approximation, replacing the fields by their expectation values, one gets a set of non-linear coupled equations:

1. The Dirac equation with potential terms involving meson and electromagnetic (e.m.) fields describing the nucleon dynamics
2. A set of Klein-Gordon type equations with sources involving nucleonic currents and densities, for mesons and the photon.

This set of equations, known as RMF equations is to be solved self - consistently. The pairing correlations, essential for the description of open shell nuclei, are incorporated either by simple BCS prescription, or self consistently through the Bogoliubov transformation. The latter leads to the Relativistic Hartree Bogoliubov (RHB) equations. The RHB equations [64] read:

$$\begin{pmatrix} h_D - \lambda & \hat{\Delta} \\ -\hat{\Delta}^* & -h_D^* + \lambda \end{pmatrix} \begin{pmatrix} U \\ V \end{pmatrix}_k = E_k \begin{pmatrix} U \\ V \end{pmatrix}_k \quad (1)$$

Here, λ is the Lagrange multiplier, E_k is the quasi-particle energy and U_k and V_k are the four dimensional Dirac spinors, normalized as:

$$\int (U_k^\dagger U_{k'} + V_k^\dagger V_{k'}) = \delta_{kk'} ; \quad (2)$$

h_D is the usual RMF Dirac Hamiltonian:

$$h_D = -\boldsymbol{\iota}\alpha \cdot \nabla + \beta(M + g_\sigma\sigma) + g_\omega\omega^o + g_\rho\tau_3\rho_3^o + e\frac{1 - \tau_3}{2}A^o \quad (3)$$

Here M is the nucleon mass, σ is the scalar field and ω^o , ρ_3^o and A^o are the Lorentz time like components of the respective meson and e.m. fields. These fields are to be determined self-consistently through the Klein-Gordon (KG) equations:

$$\{-\nabla^2 + m_\sigma^2\}\sigma = -g_\sigma\rho_s - g_2\sigma^2 - g_3\sigma^3 \quad (4)$$

$$\{-\nabla^2 + m_\omega^2\}\omega^o = g_\omega\rho_v + g_4\omega^{o\ 3} \quad (5)$$

$$\{-\nabla^2 + m_\rho^2\}\rho_3^o = g_\rho\rho_3 \quad (6)$$

$$-\nabla^2 A^o = e\rho_c \quad (7)$$

Here, m_σ (g_σ), m_ω (g_ω) and m_ρ (g_ρ) are the masses (coupling constants) of σ , ω and ρ fields respectively; g_2 is the coupling constant for the cubic self interaction terms for the σ field; g_3 (g_4) is the coupling constant for the quartic self interaction term for the σ (ω) field and e is the electronic charge. The sources (nuclear currents and densities) appearing in the above Klein-Gordon equations involve super spinors (U (V)):

$$\rho_s = \sum_{E_k > 0} V_k^\dagger \gamma^0 V_k , \quad (8)$$

$$\rho_v = \sum_{E_k > 0} V_k^\dagger V_k , \quad (9)$$

$$\rho_3 = \sum_{E_k > 0} V_k^\dagger \tau_3 V_k, \quad (10)$$

$$\rho_c = \sum_{E_k > 0} V_k^\dagger \frac{1 - \tau_3}{2} V_k \quad (11)$$

In practice, the sum in Eqs. (8 - 11) is taken over the positive energy states (no-sea approximation).

The RHB equations have two distinct parts: the self consistent field (h_D) that describes the long range particle-hole correlations and the pairing field ($\hat{\Delta}$) that accounts for the correlations in the particle-particle (pp) channel. The pairing field $\hat{\Delta}$ is expressed in terms of the matrix elements of the two body nuclear potential V^{pp} in the pp -channel and the pairing tensor involving the super-spinors (U, V). In the case of the constant gap, $\hat{\Delta}$ ($\equiv \Delta$) becomes diagonal resulting in the BCS type expressions for the occupation probabilities (v^2) [61, 64]:

$$v_k^2 = \frac{1}{2} \left[1 - \frac{\epsilon_k - \lambda}{\sqrt{(\epsilon_k - \lambda)^2 + \Delta^2}} \right] \quad (12)$$

ϵ_k being the energy of the single particle state k and the Lagrange multiplier λ (fermi energy) is to be determined through the BCS number equation. As a result, the RHB equations (Eq. 1) reduce to the RMF equations with a constant gap.

A reliable and satisfactory derivation of V^{pp} is not yet achieved in RMF [64, 77]. Therefore, in practice, it is customary to adopt a phenomenological approach while solving the RHB equations. Therefore, one often uses for V^{pp} , the finite range Gogny-D1S [78, 79] interaction, which is known to have the right pairing content and is given by:

$$V(\mathbf{r}_1, \mathbf{r}_2) = \sum_{i=1,2} e^{-\{(\mathbf{r}_1 - \mathbf{r}_2)/\mu_i\}^2} (W_i + B_i P^\sigma - H_i P^\tau - M_i P^\sigma P^\tau). \quad (13)$$

where, μ_i , W_i , B_i , H_i & M_i ($i=1,2$) are parameters of the interaction. In the case of the constant gap approximation, the required gap parameters are fixed so as to reproduce the corresponding Gogny D1S pairing energies.

Next we present and discuss the calculated ground state properties of the nuclei belonging to α - decay chains of superheavy nuclei.

4. Results and Discussions

4.1. Ground State Properties

The RMF / RHB equations are solved either using the basis expansion technique, or in coordinate space. Explicit numerical calculations require the following inputs:

- 1) The parameters appearing in the Lagrangian and
- 2) pairing gaps (or V^{pp})

The output includes Dirac spinors, single particle (quasi-particle) energies, occupancies and the mesonic and e.m. fields. These in turn are used to obtain total binding energies, radii, densities, deformations etc.

A number of Lagrangian parameter sets exist in the literature. Here, we employ the most frequently used parameter set NL3 [80]. For comparison, we also use the NL-SV1

parameter set [81] in some cases. These sets are listed in Tab. (1). In NL-SV1, the coupling constant (g_4) for the quartic self - interaction term of the isoscalar - vector ω field is also included, and its value is 41.010. This inclusion improves the equation of state of nuclear matter. It is seen that results obtained by using the other Lagrangian parameter sets (e.g. NL1 [59, 61], NL-SH [82]) exhibit similar systematics. Therefore, the inferences made and the conclusions drawn here are expected to hold for the other parameter sets as well.

In this work we solve the RMF equations in the axially symmetric deformed oscillator basis. The resulting quantities (binding energies, deformation parameters, matter radii, etc.) are denoted by NL3 / NL-SV1. The required (spherical) pairing gaps are tuned to reproduce the pairing energy obtained from RHB calculations using the Gogny D1S interaction in the pairing channel.

Table 1

The different sets of Lagrangian parameters commonly used in the RMF / RHB calculations. The masses are in MeV. All the coupling constants are dimensionless, except g_2 which is expressed in terms of fm^{-1} .

| | M | m_σ | m_ω | m_ρ | g_σ | g_ω | g_ρ | g_2 | g_3 |
|--------|-----|------------|------------|----------|------------|------------|----------|---------|---------|
| NL3 | 939 | 508.194 | 782.501 | 763 | 10.217 | 12.868 | 4.474 | -10.431 | -28.885 |
| NL-SV1 | 939 | 510.035 | 783 | 763 | 10.125 | 12.727 | 4.492 | -9.241 | -15.388 |

We now present and discuss the calculated ground state properties. The numerical values of the calculated ground state properties and the decay half lives are presented in Tab. 2.

4.1.1. Binding Energies

The calculated and the corresponding extrapolated (Audi2003) [83] binding energies for the nuclei appearing in some of the α - decay sequences of observed superheavy nuclei are presented in Fig. (1). The DEF results obtained using NL3 (NL-SV1) parameter set are denoted by NL3 (NL-SV1). It can be seen that both the calculations are in agreement with each other, and also with the corresponding Audi2003 values. However, it should be noted that the NL3 parameter set always yields a slightly deeper solution in comparison with NL-SV1. Further, both these calculations are found to yield consistently larger binding energies in comparison with the corresponding Audi2003 values. The differences, however, are small (about 5 parts in 2000).

4.1.2. Deformations

The quadrupole deformation parameters (β) are obtained from the calculated point neutron (Q_n) and proton (Q_p) quadrupole moments through:

$$Q = Q_n + Q_p = \sqrt{\frac{16\pi}{5}} \frac{3}{4\pi} AR_o^2\beta$$

with $R_o = 1.2A^{1/3}$ (fm). The calculated β for the nuclei considered are shown in Fig. (2), along with the corresponding Moller - Nix (MN) values [84]. The NL3 and NL-SV1 parameter sets yield similar deformations. These graphs reveal a number of additional interesting features. First, most of the nuclei investigated here turn out to be prolate in shape. Very few of these are spherical. These findings agree with those reported by Moller and Nix [84] with some exceptions. Further, highly deformed solutions do appear for some very heavy nuclei with both NL3 and NL-SV1 parameter sets. We note that apart from these highly deformed solutions (which happen to be the lowest), nearby solutions also exist with smaller values of β . These solutions are indicated by open / filled boxes in the respective figures for the deformation parameter β . It has been shown in the literature [85] that with the incorporation of additional constraints, e.g. the octupole, these highly deformed solutions disappear. We shall ignore these solutions, and not discuss them here.

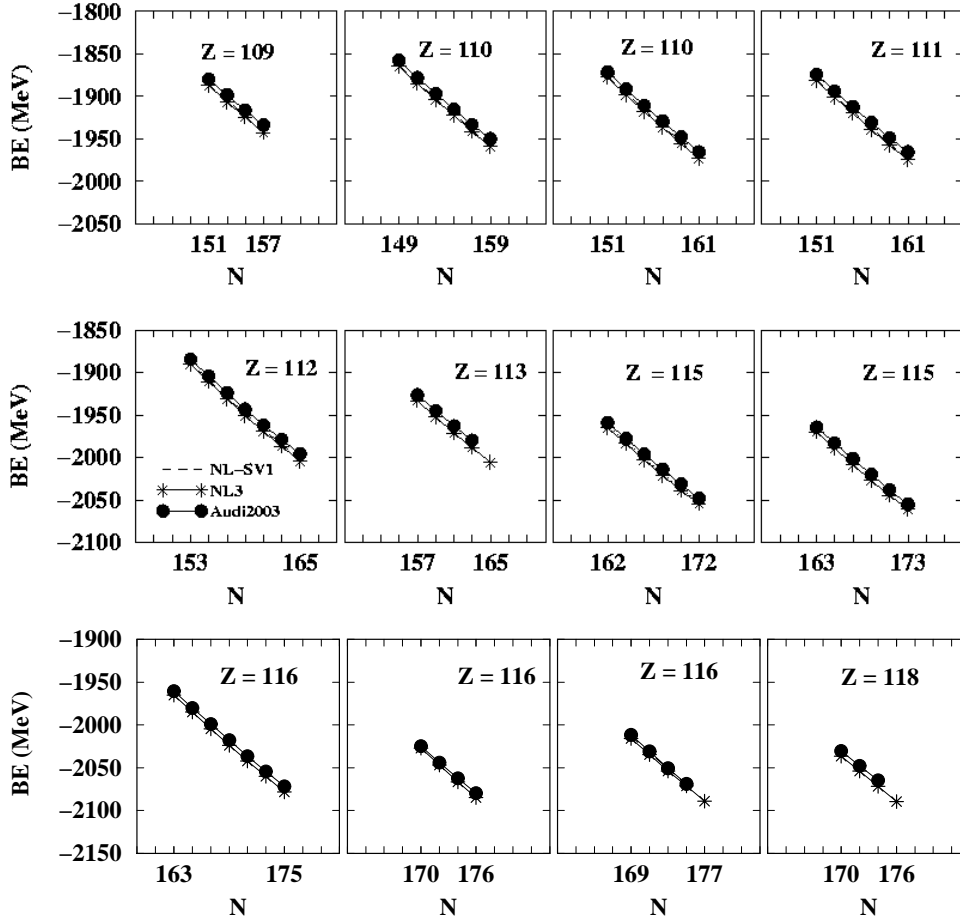


Figure 1. The calculated and the Audi2003 [83] binding energies for the nuclei belonging to α - decay chains of different superheavy nuclei.

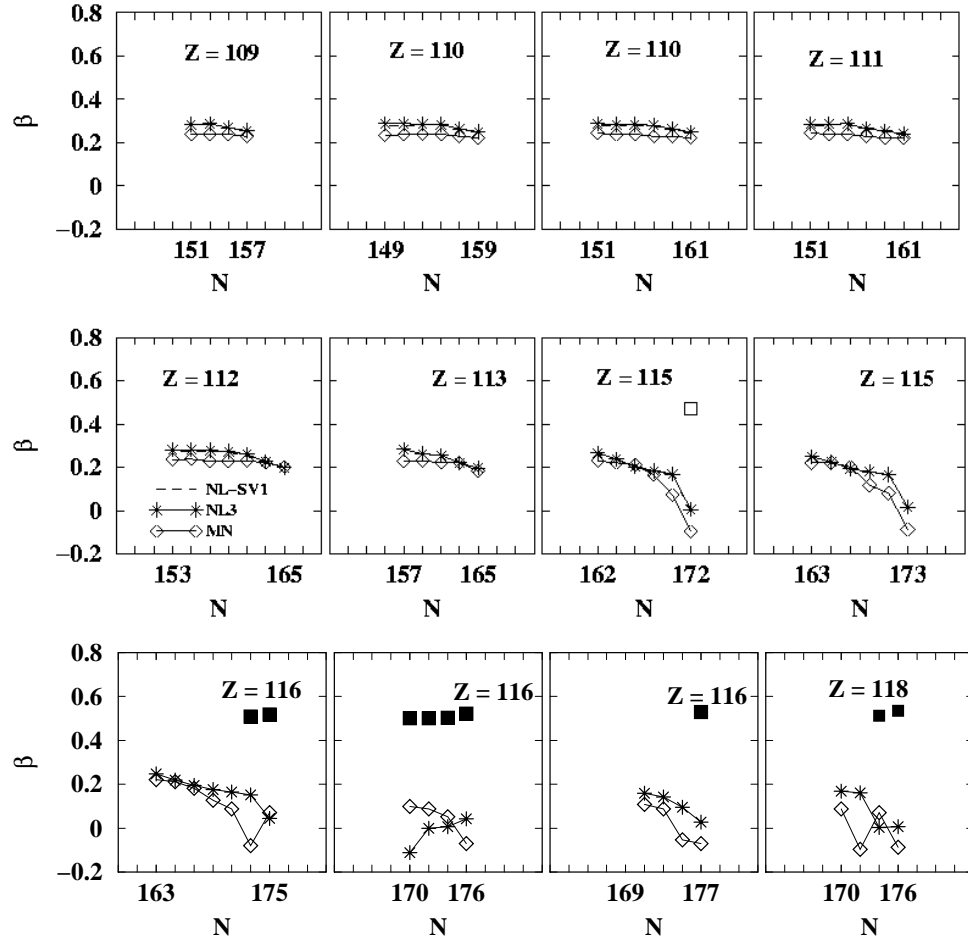


Figure 2. The quadrupole deformation parameters. The corresponding Moller - Nix values [84] are also indicated for comparison. Highly deformed solutions are indicated by open (filled) squares for NL-SV1 (NL3) results.

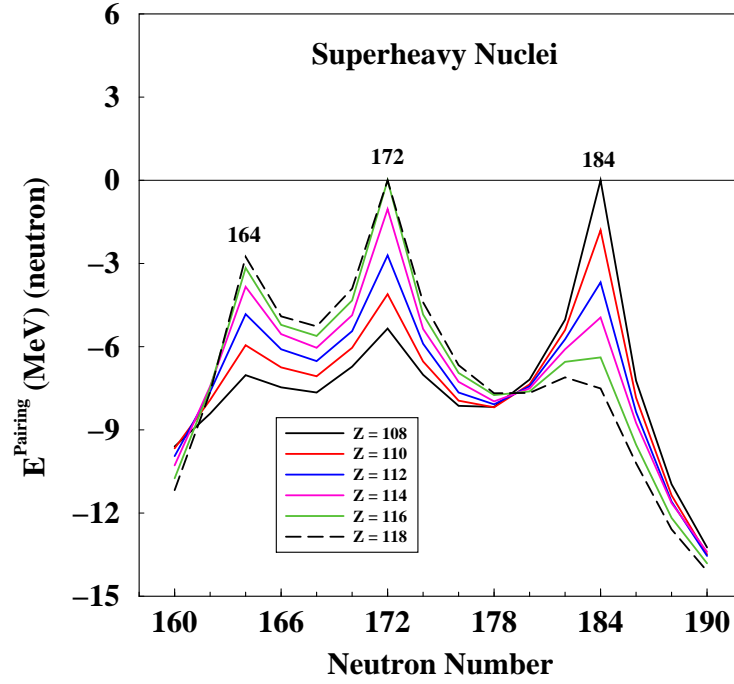


Figure 3. Neutron pairing energies for even-even nuclei in the region $108 \leq Z \leq 118$.

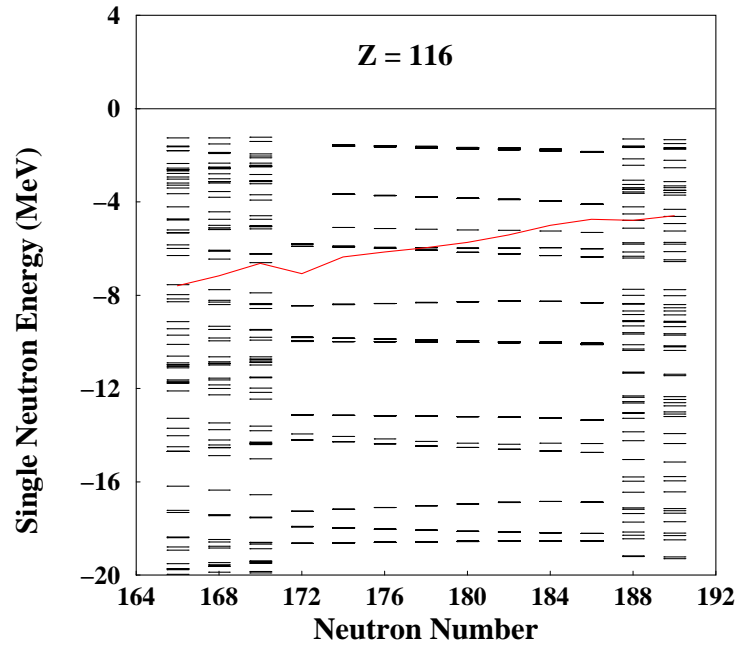


Figure 4. Single particle states for $Z = 116$ isotopes.

4.1.3. Pairing Energy

One of the characteristic features of a closed shell is the existence of a sharp maximum in the pairing energy curve. Here, we investigate the calculated D1S pairing energies for even-even nuclei in the isotopic chains of $Z = 108$ to $Z = 118$. For this purpose, the calculated neutron pairing energies corresponding to spherical solutions are shown in Fig. (3). This figure reveals that the pairing energy for $Z = 108$ at neutron number (N) 184 is zero, indicating that this neutron number may indicate shell closure for $Z = 108$. As Z increases, the pairing energy for this neutron number also increases, while the position of the peak is unchanged. Beyond $Z = 116$, however, the peak disappears, which may indicate loss of ‘magicity’. A similar ‘peak’ is observed at neutron numbers 172 and 164, where, the peak exists for all the elements considered. Further, for $Z = 116$ and 118, the pairing energy turns out to be zero. For elements lighter than $Z=116$, the pairing energy is deeper (i.e. negative) and turns out to be deepest at $Z = 108$. This analysis, therefore, indicates that the existence of such ‘magicity’ depends on the *combination* of both proton and neutron numbers rather than on either one alone. This conclusion is consistent with the findings of [66].

4.1.4. Single Particle States

Magicity can be associated with the existence of a large gap between the last occupied state and the first unoccupied state. To examine this in detail, we plot the calculated (NL3) single particle states for isotopes of element 116 in Fig. (4). The fermi levels are joined by a continuous solid line. A gap is evident at neutron number 172 ($^{288}116$). This observation is consistent with the plot of pairing energies where, at neutron number 172, the pairing energy has a sharp maximum around 0 MeV. Furthermore, the isotopes of $Z = 116$ turn out to be spherical or nearly so, in the neighborhood of neutron number 172 ($^{288}116$). This fact lends support to the conclusion that for the $Z=116$ isotopes, shell closure may be indicated at neutron number 172.

To convey the structure of the single particle levels near the Fermi surface, we display the calculated (NL3) levels in Figs. (5-7) for the nuclei appearing in the observed α - decay chains of SHE.

Table 2: The calculated ground state properties of SHE. The Q values and decay half lives are also indicated. Here, Ex+WKB represents the half lives obtained by using the experimental Q values in WKB.

| A | Z | BE/A (MeV) | | β | | r_o (fm) | Q_α (MeV) | | $\log_{10} T_\alpha$ (s) | | |
|-----|-----|------------|--------|---------|-------|---------------|------------------|-------|--------------------------|--------|-------|
| | | NL3 | Audi03 | NL3 | MN | | NL3 | Expt. | NL3 | Ex+WKB | Expt. |
| 294 | 118 | -7.11 | | 0.01 | -0.09 | 0.96 | 11.18 | 11.81 | -1.67 | -3.21 | -2.74 |
| 293 | 116 | -7.13 | | 0.03 | -0.07 | 0.96 | 10.63 | 10.69 | -0.95 | -1.12 | -1.21 |
| 292 | 116 | -7.13 | -7.12 | 0.04 | -0.07 | 0.96 | 9.91 | 10.80 | 1.16 | -1.36 | -1.74 |
| 291 | 116 | -7.14 | -7.12 | 0.04 | 0.07 | 0.96 | 11.69 | 10.89 | -3.70 | -1.72 | -2.20 |
| 290 | 116 | -7.14 | -7.12 | 0.00 | 0.07 | 0.96 | 12.00 | 11.00 | -4.33 | -1.94 | -1.82 |
| 288 | 115 | -7.15 | -7.14 | 0.02 | -0.09 | 0.96 | 12.40 | 10.61 | -5.49 | -1.23 | -1.06 |
| 287 | 115 | -7.16 | -7.14 | 0.01 | -0.10 | 0.96 | 13.05 | 10.74 | -6.79 | -1.58 | -1.49 |

continued on next page

| <i>continued from previous page</i> | | | | | | | | | | | |
|-------------------------------------|-----|------------|--------|---------|------|---------------|------------------|-------|--------------------------|--------|-------|
| A | Z | BE/A (MeV) | | β | | r_o (fm) | Q_α (MeV) | | $\log_{10} T_\alpha$ (s) | | |
| | | NL3 | Audi03 | NL3 | MN | | NL3 | Expt. | NL3 | Ex+WKB | Expt. |
| 260 | 105 | -7.38 | -7.36 | 0.29 | 0.24 | 0.97 | 9.63 | 9.34 | -1.19 | -0.86 | -0.24 |
| 258 | 105 | -7.39 | -7.36 | 0.29 | 0.24 | 0.97 | 9.33 | 9.15 | -0.77 | -0.24 | 0.46 |
| 267 | 104 | -7.36 | -7.34 | 0.25 | 0.22 | 0.97 | | | | | |
| 261 | 104 | -7.40 | -7.37 | 0.28 | 0.23 | 0.97 | 8.24 | 8.65 | 2.23 | 0.84 | 0.67 |
| 259 | 104 | -7.40 | -7.38 | 0.28 | 0.24 | 0.97 | 8.70 | 9.02 | 0.77 | -0.24 | 0.23 |
| 257 | 104 | -7.41 | -7.38 | 0.28 | 0.24 | 0.97 | 8.88 | 8.71 | 0.22 | 0.68 | 1.14 |
| 256 | 103 | -7.43 | -7.40 | 0.28 | 0.24 | 0.97 | 8.30 | 8.59 | 1.82 | 0.80 | 1.82 |
| 254 | 103 | -7.43 | -7.40 | 0.28 | 0.24 | 0.97 | | | | | |
| 257 | 102 | -7.43 | -7.41 | 0.28 | 0.24 | 0.97 | 7.59 | 8.47 | 3.93 | 0.72 | 1.18 |
| 255 | 102 | -7.44 | -7.42 | 0.28 | 0.24 | 0.97 | 7.88 | 8.06 | 2.88 | 2.27 | 1.57 |
| 253 | 102 | -7.45 | -7.42 | 0.29 | 0.24 | 0.97 | 8.05 | 8.14 | 2.37 | 1.99 | 1.63 |
| 252 | 101 | -7.46 | -7.44 | 0.28 | 0.24 | 0.97 | | | | | |
| 251 | 100 | -7.48 | -7.46 | 0.29 | 0.24 | 0.97 | | | | | |
| 253 | 100 | -7.47 | -7.45 | 0.28 | 0.24 | 0.97 | | | | | |
| 249 | 100 | -7.49 | -7.46 | 0.29 | 0.23 | 0.97 | | | | | |

4.1.5. Q Values

The Q value of a parent nucleus against α - decay is simply the difference between the binding energy of the parent nucleus and the sum of the binding energies of both the resulting daughter and α particle. Here, we present Q -values for the NL3 and NL-SV1 parameter sets in Fig. (8). Both calculations are found to be in agreement with each other, and also with the corresponding experimental values. The calculations deviate from experiment. At some places, the maximum departure is of the order of about 1 MeV, except for the decay chain on $Z = 115$, where the deviation is about 2 MeV in a few cases. This level of agreement is indeed gratifying in view of the fact that the Q value is the difference between large numbers. A small error in even one of them, could affect the Q value substantially.

4.1.6. Matter Radii

The root mean squared (rms) matter radii (r_m) are obtained from the rms proton and neutron radii through:

$$r_m^2 = \frac{Zr_p^2 + Nr_n^2}{Z + N}. \quad (14)$$

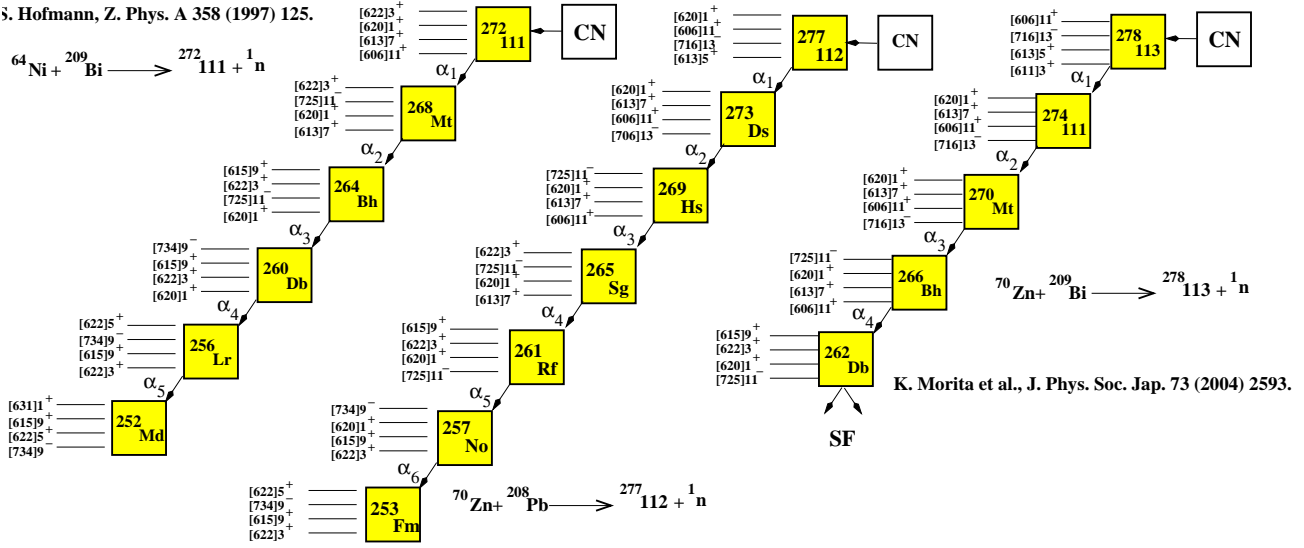
The calculated r_m values are shown in Fig. (9). The r_m values are found to be varying monotonically with mass number. The radius parameter r_o extracted using the conventional relation:

$$r_m = r_o A^{1/3} \quad (15)$$

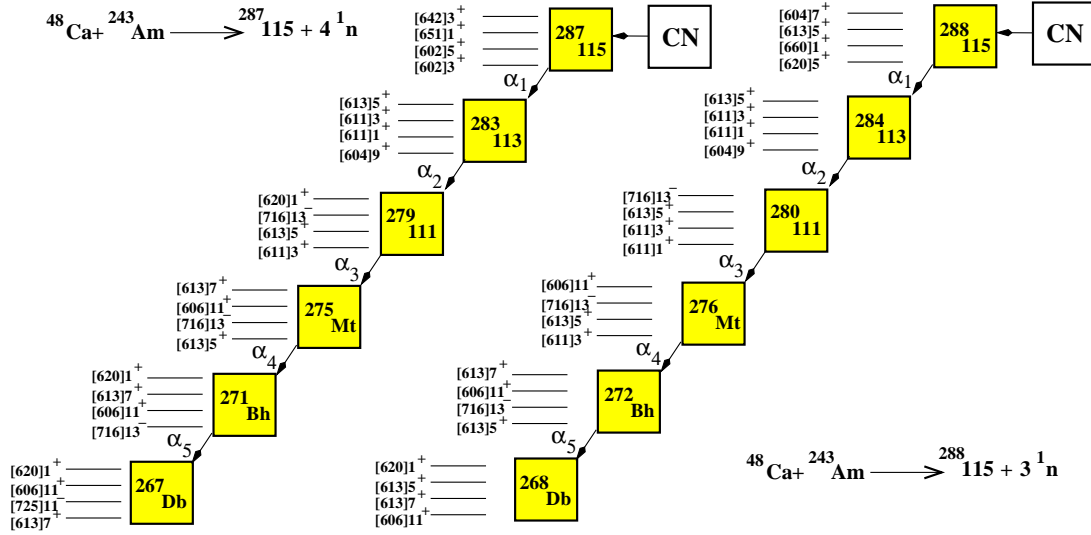
is found to be a constant ($r_o = 0.9639 \pm 0.0005$) for all the nuclei appearing in the α - decay chains of SHE, shown in figure 10.

Figure 5. Single particle level structure near the Fermi level

S. Hofmann, Z. Phys. A 358 (1997) 125.

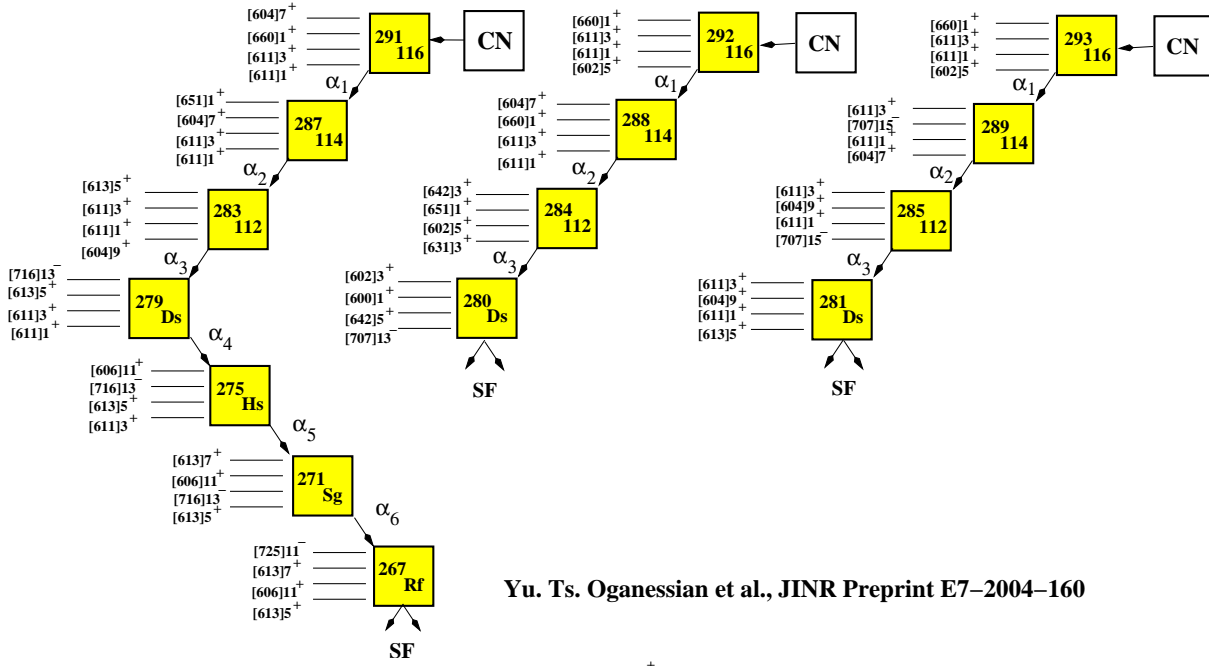


S. Hofmann et al, Z. Phys. A 354 (1996) 229.



Yu. Ts. Oganessian et al., Phys. Rev. C 69 (2004) 021601(R).

Figure 6. Single particle level structure near the Fermi level



Yu. Ts. Oganessian et al., JINR Preprint E7-2004-160

Yu. Ts. Oganessian et al., JINR Preprint E7-2004-160

Figure 7. Single particle level structure near the Fermi level

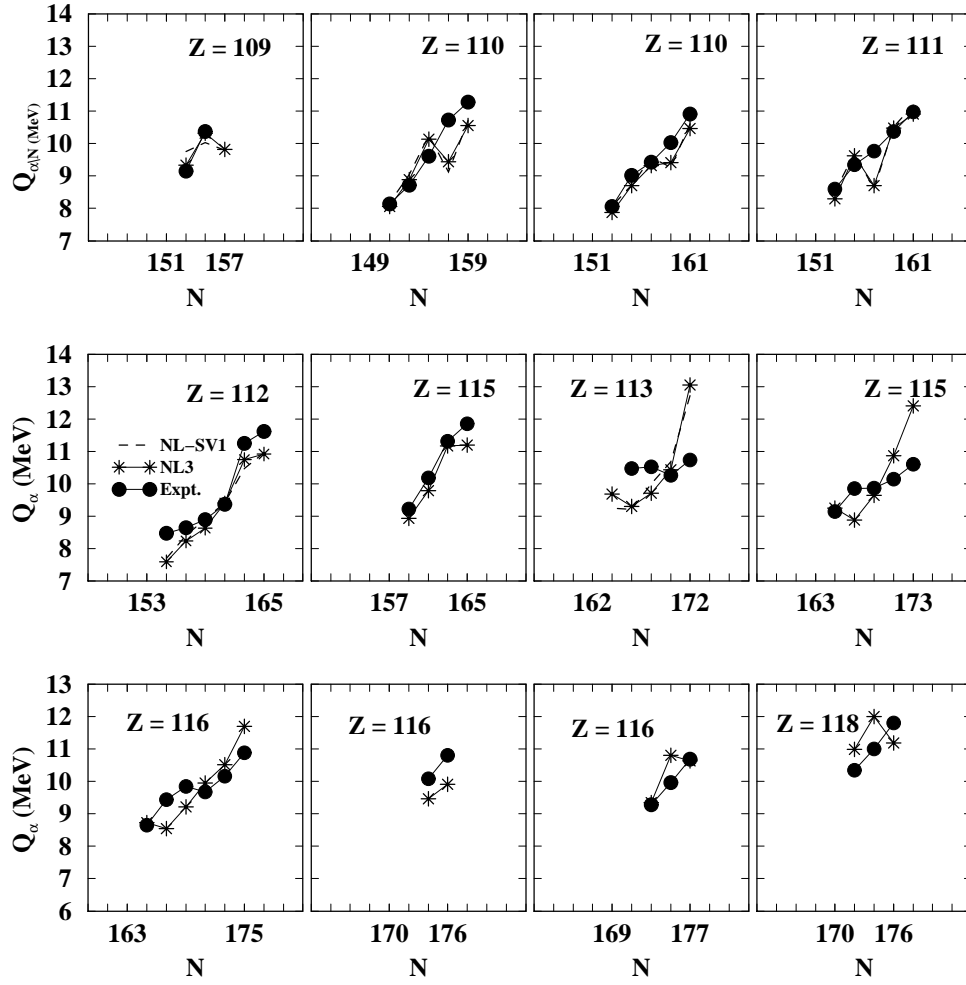
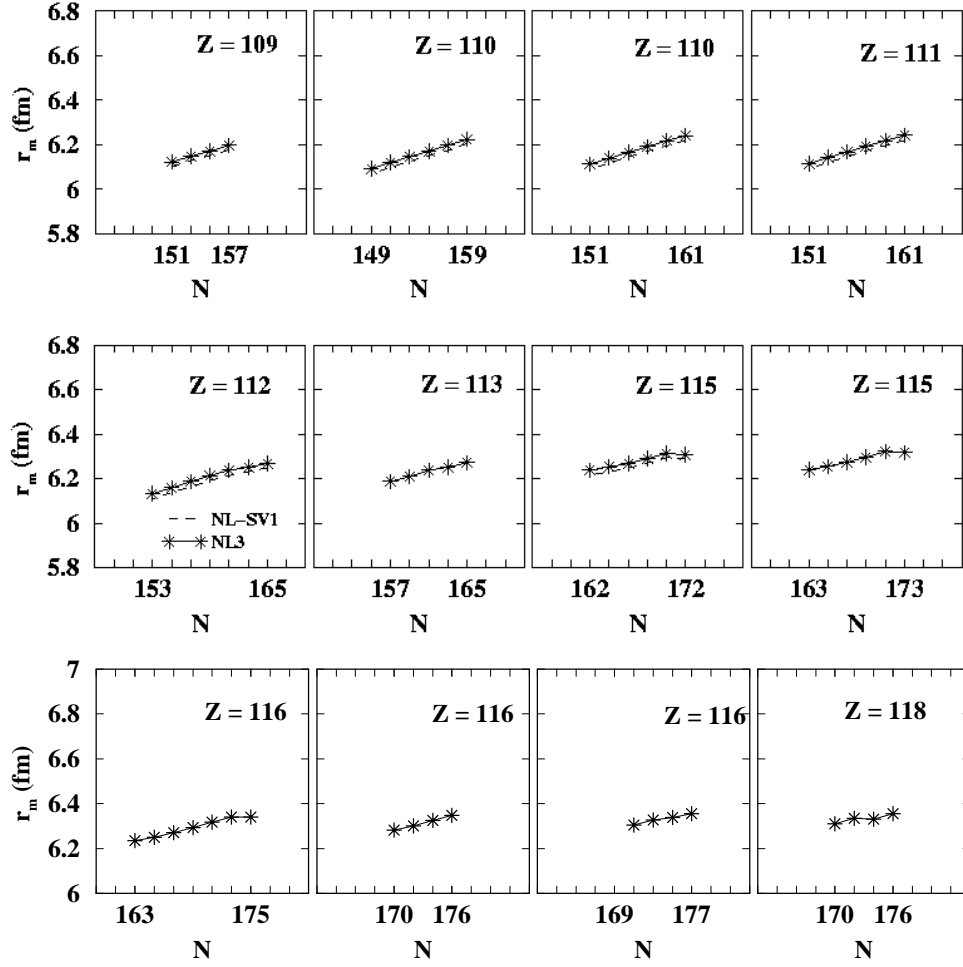
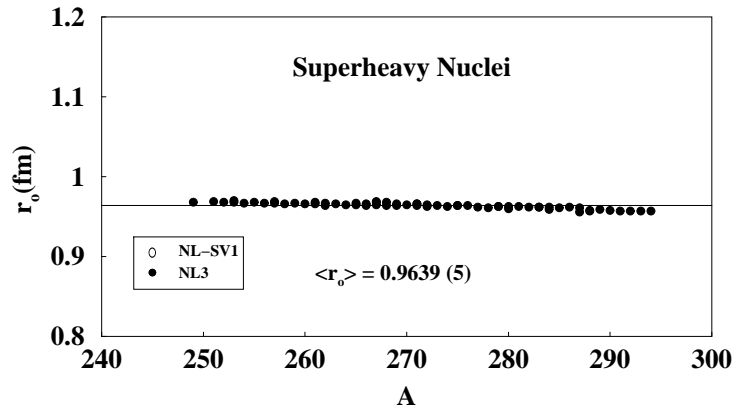


Figure 8. The Q values against α - decay. The corresponding experimental values are also shown, where available.

Figure 9. The rms matter radii.Figure 10. The extracted r_o .

4.2. Half Lives

4.2.1. Double Folding Model and WKB analysis

The basic idea behind the double folding model is to get a reasonable nucleus-nucleus potential, knowing some nucleon-nucleon interaction (e.g. M3Y interaction, etc.). In general, the double folding potential comprises of the direct and the exchange terms. The direct term contains the direct nucleon - nucleon matrix elements, whereas, the exchange term, as the name suggests, contains the exchange part. The latter is considerably more difficult to handle in practice. Thus, for some of the applications, the exchange term is *simulated* by a delta function pseudo-potential, with some density dependence.

In the present work, the double folding prescription to obtain the nucleus - nucleus potential has been used (refer to Fig. (11) for the geometry of the problem). The M3Y effective nucleon - nucleon interaction employed here is given by [86, 87, 88]:

$$v^{M3Y} = 7999 \frac{e^{-4s}}{4s} - 2134 \frac{e^{-2.5s}}{2.5s} \quad (16)$$

The exchange effects are considered only through a delta function pseudo-potential [87]:

$$v^{pseudo} = J_{00}(E)\delta(s) ; \quad (17)$$

where, the volume integral (J_{00}) is [87]:

$$J_{00} = -276 \left(1 - \frac{0.005E}{A_\alpha}\right) \text{ in MeV} - \text{fm}^3 \quad (18)$$

In the present work, the energy dependence is ignored. Thus, the M3Y interaction with pseudo-potential becomes:

$$v^{M3Y+pseudo} = 7999 \frac{e^{-4s}}{4s} - 2134 \frac{e^{-2.5s}}{2.5s} - 276\delta(s) \quad \text{in MeV} \quad (19)$$

The density dependence is supposed to compensate to some extent the higher order exchange effects and the effects of the Pauli Blocking. Following the earlier work [87], it is assumed to be of the form:

$$v^{dd} = C(1 - \beta(E)\rho_1^{2/3})(1 - \beta(E)\rho_2^{2/3}) \quad (20)$$

where, C is the overall normalization constant, and is taken to be 1.0 in the present work. $\beta(E)$ is the energy dependent part of the density dependent term and is assumed to have a constant value, 1.6 [87].

With the density dependence and the M3Y with pseudo-potential, the assumed nucleon-nucleon interaction is now given by:

$$v(s) = C \left(7999 \frac{e^{-4s}}{4s} - 2134 \frac{e^{-2.5s}}{2.5s} - 276\delta(s) \right) (1 - \beta(E)\rho_1^{2/3})(1 - \beta(E)\rho_2^{2/3}) \quad (21)$$

In these expressions, $\beta(E)$ is 1.6 and s is equal to \vec{r}_{pt} (refer to the figure).

The total double folding potential between the nucleus - nucleus system is:

$$V_{PT}(\vec{R}) = \int \rho_P(\vec{r}_p) \rho_T(\vec{r}_t) v(\vec{r}_p - \vec{r}_t + \vec{R}) d\vec{r}_p d\vec{r}_t \quad (22)$$

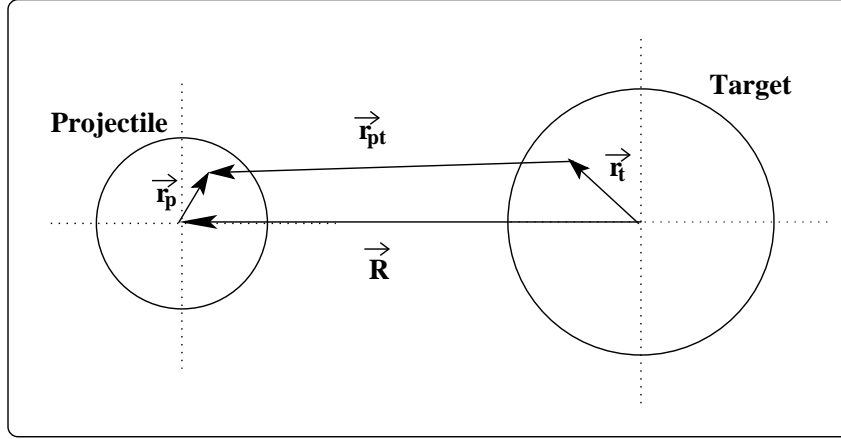


Figure 11. Geometry of the Double Folding prescription.

where, v is as defined above (Eq. (21)). In the actual calculations, we evaluate the six dimensional integral in the above equation by transforming it into the momentum space. The details are easy to work out and are straightforward.

In order to evaluate the half life time of the nucleus against α - decay, one needs to know the nuclear potential, the Coulomb potential and the energy of the alpha particle, which in turn is obtained by the Q value and the zero point energy of the oscillation of the alpha particle in the potential well. The point to be noted here is, in the present case, it is assumed that the alpha particle is already formed in the parent nucleus, so that, its motion can be simulated by assuming that it is moving in an average potential well formed by the *daughter* - α system. The Coulomb potential required in this case, is obtained by folding the point proton densities of target and projectile with the Coulomb interaction.

Here the decay half life is calculated using the WKB approximation. The half life time of the nucleus (parent) against the α - decay is then given by:

$$T_{1/2} = \frac{\ln 2}{\nu} (1 + e^K) \quad (23)$$

where, within the WKB approximation, the action integral is given by:

$$K = \frac{2}{\hbar} \int_{R_a}^{R_b} \{2\mu (E(R) - Q)\}^{1/2} dR, \quad (24)$$

and

$$E(R) = V_{PT}(R) + V_C(R) + \frac{\hbar^2 \lambda^2}{2\mu r^2}$$

The third term represents the centrifugal barrier with $\lambda = l + 1/2$, l being the orbital angular momentum. The R_a and R_b are the lower and upper turning points respectively. These are determined through the requirement:

$$E(R_a) = Q + E_\nu = E(R_b)$$

In Eq. (23), ν is the assault frequency, given by:

$$\nu = \left(\frac{1}{2R} \sqrt{\frac{2E}{M}} \right), \quad (25)$$

where, R is the radius of the parent, given by $R = 1.2A^{1/3}$; E is the energy of the alpha particle, corrected for recoil; M is mass of alpha particle, expressed in MeV.

We now present and discuss the calculated half live values.

4.2.2. Half Lives

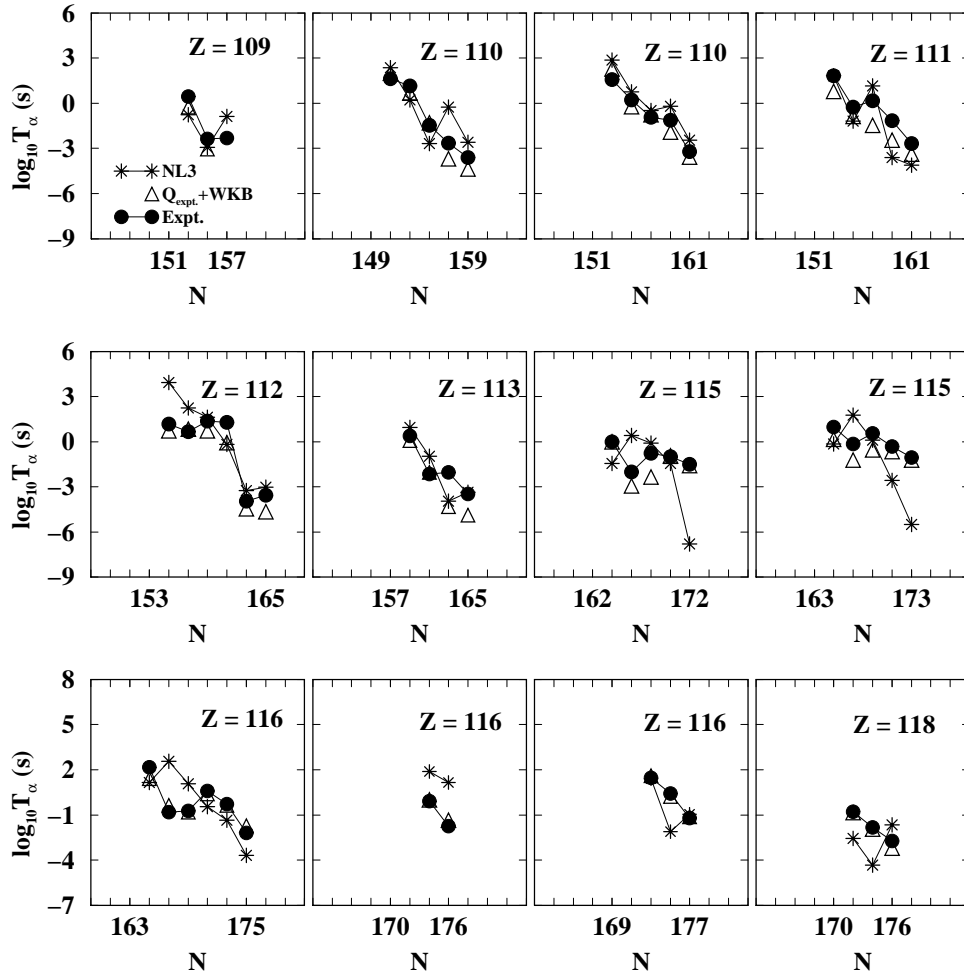


Figure 12. Half lives against α - decay of superheavy nuclei.

The calculated and the corresponding experimental half lives for the superheavy nuclei against α - decay are presented in Fig. (12). Here, we have not presented the results

for NL-SV1, since, we have already shown that the difference between NL3 and NL-SV1 results is negligible.

Results of two independent calculations have been presented in Fig. (12). In the first case, the calculated Q values are used in the WKB procedure. These results are denoted by NL3. In the second case, the experimental Q values are used in the WKB procedure, with the same microscopic potential, as in the first case. These results are denoted by $Q_{\text{expt.}} + \text{WKB}$ in Fig. (12). It is clearly seen that the use of experimental Q values in WKB approach reproduces the experimental values rather well, indicating the reliability of the microscopic nucleus - nucleus potential, and also validating the procedure that we follow in this work. The half lives obtained by using the calculated Q values, though similar to the experimental trend, differs from it quantitatively at places. This reflects hyper - sensitivity of the half lives on Q values.

5. Summary and conclusions

Extensive and systematic microscopic self consistent RMF calculations for the nuclei appearing in the α - decay chains of the known superheavy elements are presented. The RMF results with only a few (seven) fixed Lagrangian parameters are found to reproduce the corresponding experimental ground state properties remarkably well. This indeed, is gratifying. The predicted neutron shell closures $N \sim 164, 172$ and 184 are consistent with the recent experimental observations. The calculated root mean square radii closely follow the $A^{1/3}$ law.

The interaction potential between the α and daughter nucleus, obtained in the $t\rho\rho$ approximation using the RMF densities and the nucleon - nucleon interaction M3Y is employed to estimate the α - decay half lives. The calculations qualitatively agree with the experiment. The use of experimental Q values brings the calculations closer to the experiment. Therefore, the calculated interaction potential is reliable and can be used with confidence in other reaction studies.

Acknowledgments

The authors are thankful to P. Ring, M. M. Sharma, J. Meng, G. M nzenberg, S. Hoffmann, K. Morita, Yu. Ts. Oganessian, M. G. Itkis, E. M. Kozulin, E. Cherepanov, A. Sobiczewski, S. S. Kapoor and S. H. Patil for their interest in this work. Partial financial support from the Board for Research in Nuclear Sciences (BRNS), Govt. of India (Proj. No. 2001/37/13/BRNS/485) is gratefully acknowledged. MG is thankful to Department of Science and Technology (DST), Govt. of India (Proj. No. SR/WOS-A/PS-108/2003) for financial support.

REFERENCES

1. S. G. Nilsson *et al.*, Nucl. Phys. A 131 (1969) 1.
2. U. Mosel and W. Greiner, Z. Phys. A 222 (1969) 261.
3. Yu. Ts. Oganessian *et al.*, Nucl. Phys. A 701 (2002) 87c.
4. Yu. Ts. Oganessian *et al.*, Nucl. Phys. A 701 (2002) 104c.
5. A. Ghiorso *et al.*, Phys. Rev. Lett. 33 (1974) 1490.
6. P. Armbruster, Ann. Rev. Nucl. Part. Sci. 35 (1985) 135.
7. S. Hoffman and G. Munzenburg, Rev. Mod. Phys. 72 (2000) 733.

8. Yu. Ts. Oganessian, *Lecture Notes in Physics* 33 (Berlin, Springer) 221 (1974).
9. G. Munzenburg *et al.*, Z. Phys. A 315 (1984) 145.
10. G. Munzenburg *et al.*, Z. Phys. A 328 (1987) 49.
11. Yu. Ts. Oganessian *et al.*, Z. Phys. A 319 (1984) 215.
12. Yu. A. Lazarev *et al.*, Phys. Rev. Lett. 75 (1995) 1903.
13. Yu. Ts. Oganessian *et al.*, Nucl. Phys. A 682 (2001) 108.
14. S. Hoffmann *et al.*, Prog. Part. Nucl. Phys. 46 (2001) 293.
15. S. Hoffmann *et al.*, Rep. Prog. Phys. 61 (1998) 639.
16. S. Hoffmann *et al.*, Z. Phys. A 354 (1996) 229.
17. S. Hoffmann *et al.*, Z. Phys. A 350 (1995) 281.
18. S. Hoffmann *et al.*, Z. Phys. A 350 (1995) 277.
19. S. Hoffmann *et al.*, Eur. Phys. J. A 14 (2002) 147.
20. T. N. Ginter *et al.*, Phys. Rev. C 67 (2003) 064609.
21. K. Morita *et al.*, Nucl. Phys. A 734 (2004) 101.
22. K. Morita *et al.*, Eur. J. Phys., DOI:10.11.04/epja/i2003-10205-1 (2004).
23. K. Morita *et al.*, J. Phys. Soc. Japan 73 (2004) 1738.
24. K. Morita *et al.*, J. Phys. Soc. Japan 73 (2004) 2593.
25. K. Morita, Private communication (2004).
26. P. Armbruster, C. R. Physique 4 (2003) 571.
27. Yu. Ts. Oganessian *et al.*, Phys. Rev. Lett. 83 (1999) 3154.
28. Yu. Ts. Oganessian *et al.*, Phys. Rev. C 69 (2004) 021601.
29. Yu. Ts. Oganessian *et al.*, JINR Communication E7-2003-178 (2003).
30. Yu. Ts. Oganessian *et al.*, Phys. Rev. C 69 (2004) 054607 and references therein.
31. Yu. Ts. Oganessian *et al.*, Preprint JINR, D7-2002-287, (2002).
32. Yu. Ts. Oganessian *et al.*, Nucl. Phys. A 734 (2004) 109.
33. Yu. Ts. Oganessian, Rad. Phys. Chem. C 61 (2001) 259.
34. A. Türler, Eur. Phys. J. A 15 (2002) 271 and references therein.
35. R. C. Barber *et al.*, Prog. Part. Nuc. Phys. 29 (1992) 453.
36. M. Schädel (Edt.), *The Chemistry of Superheavy Elements*, Kluwer Academic Publishers, Dordrecht, 2003 and references therein.
37. Ch. Dölmann *et al.*, Nature 418 (2002) 859.
38. A. B. Yakushev *et al.*, Radiochim. Acta 89 (2001) 743.
39. A. B. Yakushev *et al.*, Radiochim. Acta 91 (2003) 433.
40. A. B. Yakushev *et al.*, Nucl. Phys. A 734 (2004) 204.
41. H. W. Gäggeler *et al.*, Nucl. Phys. A 734 (2004) 433.
42. Yu. Ts. Oganessian *et al.*, Preprint JINR, E7-2004-160, (2004) and references therein.
43. Yu. Ts. Oganessian *et al.*, JNRS 3 (2002) 217.
44. A. G. Popecko *et al.*, NIM A 510 (2003) 371.
45. Yu. Ts. Oganessian *et al.*, JINR Communication E7-2002-64, (2002).
46. Yu. Ts. Oganessian, Private communication, (2004).
47. E. K. Hyde *et al.* *The Nuclear Properties of the Heavy Elements* Vols. 1-3 Prentice Hall, 1964.
48. G. Münzenburg *et al.*, GSI Annual Report 1985, GSI-86-1, pg. 29.
49. Yu. Ts. Oganessian, *et al.*, Radiochim. Acta 37 (1984) 113.
50. P. Möller, J. R. Nix and K. -L. Kratz, At. Data Nucl. Data Tables 66 (1997) 131.

51. I. Muntian *et al.*, Acta Phys. Pol. B 34 (2003) 2073.
52. I. Muntian, Z. Patyk and A. Sobiczewski *et al.*, Phys. At. Nucl. 66 (2003) 1015.
53. S. Cwiok *et al.*, Phys. Rev. Lett. 83 (1999) 1108.
54. W. Greiner, Int. J. Mod. Phys. E 5 (1995) 1.
55. K. Rutz *et al.*, Phys. Rev. C 56 (1997) 238.
56. A. Bohr and Ben Mottelson, *Nuclear Structure II*, Benjamin NY, 1975, pg. 605.
57. J. D. Walecka, *Theoretical Nuclear and Subnuclear Physics*, Oxford University press 1995 and references cited therein.
58. B. D. Serot and J. D. Walecka, Adv. Nucl. Phys. 16 (1986) 1.
59. P. G. Reinhardt *et al.*, Z. Phys. A 323 (1986) 13; P. G. Reinhardt, Rep. Prog. Phys. 52 (1989) 439 and references cited therein.
60. Y. K. Gambhir and P. Ring, Pramana J. Phys. 32 (1989) 389.
61. Y. K. Gambhir, P. Ring and A. Thimet, Ann. Phys. (NY) 198 (1990) 132 and references cited therein.
62. B. D. Serot, Rep. Prog. Phys. 55 (1992) 1855.
63. Latha S. Warriar and Y. K. Gambhir, Phys. Rev. C 49 (1994) 871.
64. P. Ring, Prog. Part. Nucl. Phys. 37 (1996) 193 and references cited therein.
65. J. P. Maharana, Latha S. Warriar and Y. K. Gambhir, Ann. Phys. (NY) 250 (1996) 237.
66. G. A. Lalazissis *et al.*, Nucl. Phys. A 608 (1996) 202.
67. M. Bender *et al.*, Phys. Rev. C 60 (1999) 034304.
68. J. Meng and N. Takigawa, Phys. Rev. C 61 (2000) 064319.
69. M. Bender, Phys. Rev. C 61 (2000) 031302(R).
70. W. H. Long *et al.*, Phys. Rev. C 65 (2002) 047306.
71. Z. Ren *et al.*, Phys. Rev. C 67 (2003) 064302 and references therein.
72. Y. K. Gambhir *et al.*, Phys. Rev. C 68 (2003) 044316.
73. L. S. Geng *et al.*, arXiv:nucl-th/0310032 v2, 14 Oct 2003.
74. T. Sil *et al.*, Phys. Rev. C 69 (2004) 044315.
75. Y. K. Gambhir, A. Bhagwat and M. Gupta, Phys. Rev. C 71 (2005) 037301.
76. R. Smolanczuk and A. Sobiczewski, *Low Energy Nuclear Dynamics* 313 (1995), World Scientific Publishing Co., Singapore.
77. H. Kucharek and P. Ring, Z. Phys. A 339 (1991) 23.
78. J. F. Berger, M. Girod, and D. Gogny, Nucl. Phys. A 428 (1984) 32 (1984).
79. T. Gonzalez-Llarena *et al.*, Phys. Lett. B 379 (1996) 13.
80. G. A. Lalazissis, J. König and P. Ring, Phys. Rev. C 55 (1997) 540.
81. M. M. Sharma, A. R. Farhan and S. Mythili, Phys. Rev. C 61 (2000) 054306.
82. M. M. Sharma, M. A. Nagarajan and P. Ring, Phys. Lett. B 312 (1993) 377.
83. G. Audi *et al.*, Nucl. Phys. A 565 (2003) 1.
84. P. Möller *et al.*, At. Data Nucl. Data Tables 59 (1995) 185.
85. I. Muntian and A. Sobiczewski, Phys. Lett. B 586 (2004) 254 and references cited therein.
86. G. R. Satchler and W. G. Love, Phys. Reports 55 (1979) 183.
87. A. K. Choudhuri, Nucl. Phys. A 449 (1986) 243.
88. D. T. Khoa, W. von Oertzen and H. G. Bohlen, Phys. Rev. C 49 (1994) 1652.